Spatio-angular transfer functions for fluorescence microscopes

Talon Chandler, Min Guo, Hari Shroff, Rudolf Oldenbourg, Patrick La Rivière

April 17, 2018

Abstract

We investigate how the orientation and position of fluorescent dipole emitters affects microscopic imaging using electromagnetic optics theory. Starting with the thoroughly studied spatio-angular point spread function, we introduce the spatio-angular coherent spread function, coherent transfer function, and optical transfer function as electromagnetic extensions of well-known functions in scalar optics theory. We use these concepts to show that fluorescence microscopes have a spatio-angular band limit.

1 Introduction

We use plain roman type for scalars, e.g., x, y, z; bold lowercase roman type for two-dimensional vectors, e.g., $\mathbf{r}$; hats for unit vectors, e.g., $\hat{\mathbf{s}}$; and bold capital roman type for matrices, e.g., $\mathbf{R}$. We use the real spherical harmonic functions

$$y_l^m(\vartheta,\varphi) = \begin{cases} \sqrt{2}K_l^m \cos(m\varphi) P_l^m(\cos\vartheta), & m > 0 \\ K_l^0 P_l^0(\cos\vartheta), & m = 0 \\ \sqrt{2}K_l^m \sin(-m\varphi) P_l^{-m}(\cos\vartheta), & m < 0 \end{cases} \tag{1}$$

where

$$K_l^m = \sqrt{\frac{(2l+1)}{4\pi}\frac{(l-|m|)!}{(l+|m|)!}}, \tag{2}$$

and $P_l^m(x)$ are the associated Legendre polynomials. The $l = 0$ and $l = 1$ spherical harmonics are given by

$$\begin{gathered} y_0^0(\vartheta,\varphi) = \sqrt{\frac{1}{4\pi}}, \\ y_1^{-1}(\vartheta,\varphi) = \sqrt{\frac{3}{4\pi}}\sin\varphi\sin\vartheta, \qquad y_1^0(\vartheta,\varphi) = \sqrt{\frac{3}{4\pi}}\cos\vartheta, \qquad y_1^1(\vartheta,\varphi) = \sqrt{\frac{3}{4\pi}}\cos\varphi\sin\vartheta. \end{gathered} \tag{3}$$

2 Spatio-angular point spread functions

Figure 1 shows a schematic of the fluorescence microscope that we are considering with a summary of our notation. We start by following Backer and Moerner [1] to find the electric field at position $\mathbf{r}_b$ in the back focal plane due to a single dipole emitter at position $\mathbf{r}_o$ oriented along $\hat{\mathbf{s}}_o$ as

$$\tilde{\mathbf{e}}_b(\mathbf{r}_b;\mathbf{r}_o,\hat{\mathbf{s}}_o) \propto \mathrm{e}^{-i(kn_o/f_o)\mathbf{r}_b\cdot\mathbf{r}_o}\sqrt{\frac{1}{\rho_b}}\begin{bmatrix} \sin^2\phi_b + \rho_b\cos^2\phi_b & \sin\phi_b\cos\phi_b(\rho_b-1) & -\frac{r_b}{f_o}\cos\phi_b \\ \sin\phi_b\cos\phi_b(\rho_b-1) & \cos^2\phi_b + \rho_b\sin^2\phi_b & -\frac{r_b}{f_o}\sin\phi_b \\ 0 & 0 & 0 \end{bmatrix}\begin{bmatrix} \cos\varphi_o\sin\vartheta_o \\ \sin\varphi_o\sin\vartheta_o \\ \cos\vartheta_o \end{bmatrix}\Pi\left(\frac{r_b}{r_b^{\max}}\right), \tag{4}$$

where we define $\rho_b \equiv \sqrt{1-\left(\frac{r_b}{f_o}\right)^2}$, and $\Pi(x)$ is a boxcar function that returns 1 when $|x| < 1$ and 0 otherwise. We can understand this expression term by term—the exponential term accounts for the phase as dipole emitter is moved in object space, the square root term conserves power before and after the objective lens, the matrix models the dipole emission process and electric field rotation caused by the objective lens, the vector is the

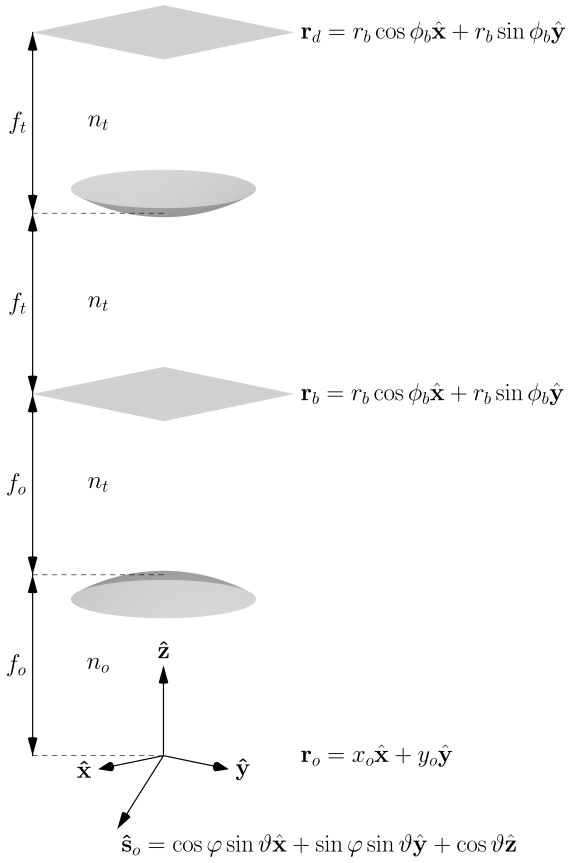

Figure 1: Simplified schematic of a single-view fluorescence microscope. The object is placed near the focal point of an aplanatic objective lens with focal length f_o in a medium with refractive index n_o. The object is parameterized by the 2D position vector $\mathbf{r}_o$ (o for object) and an orientation unit vector $\hat{\mathbf{s}}_o$. The light emitted by the fluorescent object is collected and collimated by the objective lens so that the electric fields are purely transverse in the back focal plane. Points in the back focal plane are parameterized by a 2D position vector $\mathbf{r}_b$ (b for back focal plane). Finally, the tube lens with focal length f_t refocuses the light onto a detector. Points on the detector are parameterized by a 2D position vector $\mathbf{r}_d$ (d for detector). The back focal plane and detector are in a medium with refractive index n_t. Note that this schematic is not to scale—we consider the case where $f_o \ll f_t$.

dipole orientation unit vector, and $\Pi\left(\frac{r_b}{r_b^{\max}}\right)$ accounts for the numerical aperture of the lens with $r_b^{\max} = \frac{f_0}{n_0}\text{NA}$. We use a tilde to mark single dipole response functions—we will consider the response due to a field of dipoles in the next section.

Although we will not use the result immediately, we can write the electric field in the back focal plane under the paraxial approximation. We expand Eq. 4 in a Taylor series about $r_b = 0$ and drop all second-order and higher terms to find

$$\tilde{\mathbf{e}}_b^{(p)}(\mathbf{r}_b; \mathbf{r}_o, \hat{\mathbf{s}}_o) \propto \mathrm{e}^{-i(kn_o/f_o)\mathbf{r}_b \cdot \mathbf{r}_o} \begin{bmatrix} 1 & 0 & -\frac{r_b}{f_o}\cos\phi_b \\ 0 & 1 & -\frac{r_b}{f_o}\sin\phi_b \\ 0 & 0 & 0 \end{bmatrix} \begin{bmatrix} \cos\varphi_o \sin\vartheta_o \\ \sin\varphi_o \sin\vartheta_o \\ \cos\vartheta_o \end{bmatrix} \Pi\left(\frac{r_b}{r_b^{\max}}\right). \tag{5}$$

We will continue to use a superscript (p) to mark terms that have used the paraxial approximation.

If the tube lens is weakly focusing ($f_o \ll f_t$) then we can find the electric field in the detector plane by

taking the Fourier transform of the electric field in the back focal plane

$$\tilde{\mathbf{e}}_d(\mathbf{r}_d;\mathbf{r}_o,\hat{\mathbf{s}}_o) \propto \int_{\mathbb{R}^2} d\mathbf{r}_b\, \tilde{\mathbf{e}}_b(\mathbf{r}_b;\mathbf{r}_o,\hat{\mathbf{s}}_o)\mathrm{e}^{-i(kn_t/f_t)\mathbf{r}_b\cdot\mathbf{r}_d}. \tag{6}$$

By isolating the phase term in Eq. 4 with $\tilde{\mathbf{e}}_b(\mathbf{r}_b;\mathbf{r}_o,\hat{\mathbf{s}}_o) \equiv \mathrm{e}^{-i(kn_o/f_o)\mathbf{r}_b\cdot\mathbf{r}_o}\underline{\tilde{\mathbf{e}}}_b(\mathbf{r}_b;\hat{\mathbf{s}}_o)$, and plugging into Eq. 6 we find that

$$\tilde{\mathbf{e}}_d(\mathbf{r}_d - M\mathbf{r}_o,\hat{\mathbf{s}}_o) \propto \int_{\mathbb{R}^2} d\mathbf{r}_b\, \underline{\tilde{\mathbf{e}}}_b(\mathbf{r}_b;\hat{\mathbf{s}}_o)\mathrm{e}^{-i(kn_t/f_t)\,\mathbf{r}_b\cdot[\mathbf{r}_d - M\mathbf{r}_o]}. \tag{7}$$

where $M = -\frac{n_o}{n_t}\frac{f_t}{f_o}$ is the transverse magnification. By writing the electric field in the detector plane in terms of $\mathbf{r}_d - M\mathbf{r}_o$, we have established that the electric field in the detector plane is *transverse shift-invariant*—a transverse shift of the object creates a magnified transverse shift of the image. We define coordinates on the detector centered on the image of the object $\mathbf{r}'_d \equiv \mathbf{r}_d - M\mathbf{r}_o = r'_d\cos\phi'_d\hat{\mathbf{x}} + r'_d\sin\phi'_d\hat{\mathbf{y}}$, then we follow Novotny [2] by writing the integrals in polar coordinates, evaluating the azimuthal integrals, and writing the result concisely in terms of three radial integrals

$$\tilde{\mathbf{e}}_d(\mathbf{r}'_d,\hat{\mathbf{s}}_o) \propto \begin{bmatrix} a(r'_d)+c(r'_d)\cos(2\phi'_d) & c(r'_d)\sin(2\phi'_d) & 2ib(r'_d)\cos\phi'_d \\ c(r'_d)\sin(2\phi'_d) & a(r'_d)-c(r'_d)\cos(2\phi'_d) & 2ib(r'_d)\sin\phi'_d \\ 0 & 0 & 0 \end{bmatrix} \begin{bmatrix} \cos\varphi_o\sin\vartheta_o \\ \sin\varphi_o\sin\vartheta_o \\ \cos\vartheta_o \end{bmatrix}, \tag{8}$$

where $a(r'_d), b(r'_d)$, and $c(r'_d)$ are

$$a(r'_d) = \int_0^{\theta_{\max}} d\theta\ \sqrt{\cos\theta}\sin\theta(1+\cos\theta)J_0(k_b r'_d\sin\theta f_o/f_t), \tag{9}$$

$$b(r'_d) = \int_0^{\theta_{\max}} d\theta\ \sqrt{\cos\theta}\sin^2\theta J_1(k_b r'_d\sin\theta f_o/f_t), \tag{10}$$

$$c(r'_d) = \int_0^{\theta_{\max}} d\theta\ \sqrt{\cos\theta}\sin\theta(1-\cos\theta)J_2(k_b r'_d\sin\theta f_o/f_t). \tag{11}$$

We can identify Eq. 8 as the vector-valued *coherent spread function* (CSF) of the microscope. The more familiar scalar-valued CSF—sometimes called the amplitude transfer function—is only applicable to cases where electromagnetic optics plays no role in the microscope—not true for samples that contain dipole emitters.

To build our intuition about the CSF, we will rewrite the matrix multiplication in Eq. 8 in terms of the spherical harmonics. Notice that the $l = 1$ spherical harmonics are the Cartesian components of the unit dipole axis (see Eq. 3), so the CSF becomes

$$\tilde{\mathbf{e}}_d(\mathbf{r}'_d,\hat{\mathbf{s}}_o) \propto \begin{bmatrix} [a(r'_d)+c(r'_d)\cos(2\phi'_d)]y_1^1(\hat{\mathbf{s}}_o) + c(r'_d)\sin(2\phi'_d)y_1^{-1}(\hat{\mathbf{s}}_o) + 2ib(r'_d)\cos\phi'_d y_1^0(\hat{\mathbf{s}}_o) \\ c(r'_d)\sin(2\phi'_d)y_1^1(\hat{\mathbf{s}}_o) + [a(r'_d)-c(r'_d)\cos(2\phi'_d)]y_1^{-1}(\hat{\mathbf{s}}_o) + 2ib(r'_d)\sin\phi'_d y_1^0(\hat{\mathbf{s}}_o) \\ 0 \end{bmatrix}. \tag{12}$$

By applying the paraxial approximation ($\sin\theta \approx \theta$ and $\cos\theta \approx 1$), the integrals $a(r'_d), b(r'_d)$ and $c(r'_d)$ can be evaluated in terms of Bessel functions. We can evaluate $a(r'_d)$ and $b(r'_d)$ with the help of $\int_0^z dx\ xJ_0(ax) = zJ_1(az)/a$ and $\int_0^z dx\ x^2J_1(ax) = z^2J_2(az)/a$, respectively, and $c(r'_d) = 0$ because $J_2(x)$ is zero to first order. In this case, the CSF simplifies to

$$\tilde{\mathbf{e}}_d^{(p)}(\mathbf{r}'_d,\hat{\mathbf{s}}_o) \propto \begin{bmatrix} a^{(p)}(r'_d)y_1^1(\hat{\mathbf{s}}_o) + 2ib^{(p)}(r'_d)\cos\phi'_d y_1^0(\hat{\mathbf{s}}_o) \\ a^{(p)}(r'_d)y_1^{-1}(\hat{\mathbf{s}}_o) + 2ib^{(p)}(r'_d)\sin\phi'_d y_1^0(\hat{\mathbf{s}}_o) \\ 0 \end{bmatrix}, \tag{13}$$

where the integrals evaluate to

$$a^{(p)}(r'_d) = \frac{J_1(2\pi\nu_o r'_d)}{\pi\nu_o r'_d}, \qquad b^{(p)}(r'_d) = \frac{\mathrm{NA}}{n_o}\left[\frac{J_2(2\pi\nu_o r'_d)}{\pi\nu_o r'_d}\right], \tag{14}$$

and we have substituted

$$\nu_o \equiv \frac{\mathrm{NA}}{M\lambda}, \qquad \mathrm{NA} \equiv n_o \sin\theta_{\max}. \tag{15}$$

Under the paraxial approximation the electric fields on the detector created by a single dipole are composed of two parts, a parallel part and a radial part. The coefficients of the y_1^0 spherical harmonic in Eq. 13 create the radial part of the field—the z component of the dipole generates a radial field on the detector with respect to the image point. The coefficients of the y_1^1 and y_1^{-1} spherical harmonics create a parallel field in the detector plane parallel to the x and y components of the dipole. As the NA increases and the paraxial approximation no longer applies, we begin to see coupling between the x and y components of the dipole with the y and x transverse fields, respectively.

We can find the intensity in the detector plane due to a single dipole by taking the squared modulus of the CSF

$$h(\mathbf{r}'_d, \hat{\mathbf{s}}_o) = \left|\tilde{\mathbf{e}}_d(\mathbf{r}'_d, \hat{\mathbf{s}}_o)\right|^2. \tag{16}$$

For convenience we keep the CSF written in terms of the spherical harmonics and use a table of spherical harmonic products (see Appendix A) to calculate the intensity in the detector plane as

$$\begin{aligned} h(\mathbf{r}'_d, \hat{\mathbf{s}}_o) \propto{}& \left(a^2(r'_d) + 2b^2(r'_d) + c^2(r'_d)\right) y_0^0(\hat{\mathbf{s}}_o) - \frac{2\sqrt{15}}{5} a(r'_d)c(r'_d)\sin(2\phi'_d) y_2^{-2}(\hat{\mathbf{s}}_o) \\ &+ \frac{1}{\sqrt{5}}\left(-a^2(r'_d) + 4b^2(r'_d) - c^2(r'_d)\right) y_2^0(\hat{\mathbf{s}}_o) + \frac{2\sqrt{15}}{5} a(r'_d)c(r'_d)\cos(2\phi'_d) y_2^2(\hat{\mathbf{s}}_o). \end{aligned} \tag{17}$$

We can identify Eq. 17 as the spatio-angular *point spread function* (PSF) of the microscope. Writing the spatio-angular PSF in terms of spherical harmonic functions has two advantages. First, it allows us to express the spatio-angular PSF very concisely. Instead of considering the point spread function for every possible dipole orientation, we only need to consider four spatio-angular PSFs—one for each spherical harmonic. Second, the spherical harmonic functions form an orthonormal basis for functions on the sphere—a convenient fact that we will use later.

It is useful to compare Eq. 17 to Backer and Moerner's approach [1]. They expand the spatio-angular PSF in terms of six second moments of the fluorophore distribution $\{s_x^2, s_y^2, s_z^2, s_x s_y, s_x s_z, s_y s_z\}$. This approach is very useful—only six precomputed spatio-angular PSFs are required to represent an arbitrary spatio-angular PSF. Instead of expanding in terms of six second moments, we expand onto just four spherical harmonics which, unlike the second moments, are orthonormal functions. In the next section we will use the orthonormality of the spherical harmonics to derive spatio-angular transfer functions for fluorescence microscopes.

The spatio-angular PSF under the paraxial approximation is given by

$$h^{(p)}(\mathbf{r}'_d, \hat{\mathbf{s}}_o) \propto \left(a^{(p)^2}(r'_d) + 2b^{(p)^2}(r'_d)\right) y_0^0(\hat{\mathbf{s}}_o) + \frac{1}{\sqrt{5}}\left(-a^{(p)^2}(r'_d) + 4b^{(p)^2}(r'_d)\right) y_2^0(\hat{\mathbf{s}}_o). \tag{18}$$

We rewrite the PSF in the following form to make plotting and interpretation easier

$$h^{(p)}(\mathbf{r}'_d, \hat{\mathbf{s}}_o) = h_0^{0(p)}(\mathbf{r}'_d) y_0^0(\hat{\mathbf{s}}_o) + h_2^{0(p)}(\mathbf{r}'_d) y_2^0(\hat{\mathbf{s}}_o), \tag{19}$$

$$h_0^{0(p)}(\mathbf{r}'_d) \equiv a^{(p)^2}(r'_d) + 2b^{(p)^2}(r'_d), \tag{20}$$

$$h_2^{0(p)}(\mathbf{r}'_d) \equiv \frac{1}{\sqrt{5}}\left[-a^{(p)^2}(r'_d) + 4b^{(p)^2}(r'_d)\right]. \tag{21}$$

First, consider the coefficient on the y_0^0 spherical harmonic in Eq. 18. This coefficient is the point spread function for an angularly uniform distribution of fluorophores. The first term of the coefficient ${A^{(p)}}^2(r'_d)$ is the familiar Airy disk that arises from the contribution of dipoles oriented in the transverse plane, while the second term ${B^{(p)}}^2(r'_d)$ is a smaller factor that arises from dipoles oriented outside of the transverse plane. This leads to an interesting conclusion—a uniform distribution of dipoles has a point spread function that is slightly wider than an Airy disk even in the paraxial approximation. The Airy disk is usually derived using paraxial scalar optics while here we have used paraxial electromagnetic optics. Therefore, we can consider the second term to be an electromagnetic correction to the Airy disk. We will quantify this difference in the next section.

Next, consider the coefficient on the y_2^0 spherical harmonic in Eq. 18. This coefficient is the spatial PSF for a distribution of fluorophores proportional to $3\cos^2\vartheta_o - 1$. Counterintuitively, this fluorophore distribution cannot exist because it would require a negative number of fluorophores along some orientations; but if this distribution could exist, then this coefficient would be its spatial PSF. Considering negative distributions of fluorophores in our calculations should not be cause for concern. The spherical harmonics span the space of functions on the sphere, so any positive fluorophore distribution can be represented by the spherical harmonics and we never need to consider negative fluorophores.

Finally, consider all of the spherical harmonics that have a zero coefficient. These spherical harmonics span the angular null space of our measurement system—fluorophore distributions that lie in the null space do not affect the measured intensities. Under the paraxial approximation all of the non-zero coefficients are rotationally symmetric ($m = 0$) spherical harmonics, which means that the transverse orientation of the dipoles does not affect the PSF. In the high NA case this is no longer true—two $m = 2$ spherical harmonics have non-zero coefficients and the transverse orientation of dipoles does affect the PSF.

3 Spatio-angular transfer functions

Consider a thin object that consists of fluorescent dipoles in arbitrary positions and orientations. We can represent the entire object using a function $\boldsymbol{\mu}(\mathbf{r}_o, \hat{\mathbf{s}}_o)$ that returns a complex-valued vector for each position $\mathbf{r}_o$ and direction $\hat{\mathbf{s}}_o$. The magnitude of the complex-valued vector is the magnitude of the dipole moment and the elements of the vector give the orientation and phase of the radiating dipole moment. Because $\boldsymbol{\mu}(\mathbf{r}_o, \hat{\mathbf{s}}_o)$ includes the relative phases of different points and orientations in the object, $\boldsymbol{\mu}(\mathbf{r}_o, \hat{\mathbf{s}}_o)$ can represent coupled dipoles that are emitting partially or completely coherently.

We can find the electric field on the detector created by this object by multiplying $\boldsymbol{\mu}(\mathbf{r}_o, \hat{\mathbf{s}}_o)$ with the CSF then integrating over all positions and orientations in the object

$$\mathbf{e}_d(\mathbf{r}_d) = \int_{\mathbb{S}^2} d\hat{\mathbf{s}}_o \int_{\mathbb{R}^2} d\mathbf{r}_o \; \tilde{\mathbf{e}}_d(\mathbf{r}_d - M\mathbf{r}_o, \hat{\mathbf{s}}_o)\boldsymbol{\mu}(\mathbf{r}_o, \hat{\mathbf{s}}_o). \tag{22}$$

Note that these integrals represent a vector sum—the coherence of the electric fields radiated by the object can cause cancellations of the fields created on the detector.

We can simplify this expression by expanding the CSF in terms of spatio-angular harmonics

$$\tilde{\mathbf{e}}_d(\mathbf{r}_d - M\mathbf{r}_o, \hat{\mathbf{s}}_o) = \sum_{l=0}^{\infty} \sum_{m=-l}^{l} \int_{\mathbb{R}^2} d\boldsymbol{\nu} \, \mathbf{E}_l^m(\boldsymbol{\nu}) y_l^m(\hat{\mathbf{s}}_o) \, \mathrm{e}^{i2\pi(\mathbf{r}_d - M\mathbf{r}_o)\cdot\boldsymbol{\nu}}, \tag{23}$$

where $\mathbf{E}_l^m(\boldsymbol{\nu})$ is the spatio-angular spectrum of the CSF given by

$$\mathbf{E}_l^m(\boldsymbol{\nu}) \equiv \int_{\mathbb{S}^2} d\hat{\mathbf{s}}_o \int_{\mathbb{R}^2} d\mathbf{r}_o \, \tilde{\mathbf{e}}_d(\mathbf{r}_d - M\mathbf{r}_o, \hat{\mathbf{s}}_o) y_l^m(\hat{\mathbf{s}}_o) \, \mathrm{e}^{-i2\pi(\mathbf{r}_d - M\mathbf{r}_o)\cdot\boldsymbol{\nu}}. \tag{24}$$

We can change variables to make this expression easier to evaluate

$$\mathbf{E}_l^m(\boldsymbol{\nu}) \propto \int_{\mathbb{S}^2} d\hat{\mathbf{s}}_o \int_{\mathbb{R}^2} d\mathbf{r}_o \, \tilde{\mathbf{e}}_d(\mathbf{r}'_d, \hat{\mathbf{s}}_o) y_l^m(\hat{\mathbf{s}}_o) \, \mathrm{e}^{-i2\pi\mathbf{r}'_d\cdot\boldsymbol{\nu}}. \tag{25}$$

By plugging Eq. 23 into Eq. 22 we find that

$$\mathbf{e}_d(\mathbf{r}_d) = \int_{\mathbb{S}^2} d\hat{\mathbf{s}}_o \int_{\mathbb{R}^2} d\mathbf{r}_o \left[\sum_{l=0}^{\infty} \sum_{m=-l}^{l} \int_{\mathbb{R}^2} d\boldsymbol{\nu}\, \mathbf{E}_l^m(\boldsymbol{\nu}) y_l^m(\hat{\mathbf{s}}_o)\, \mathrm{e}^{i2\pi(\mathbf{r}_d - M\mathbf{r}_o)\cdot\boldsymbol{\nu}} \right] \boldsymbol{\mu}(\mathbf{r}_o, \hat{\mathbf{s}}_o). \tag{26}$$

We can rearrange this equation into the following form

$$\mathbf{e}_d(\mathbf{r}_d) = \sum_{l=0}^{\infty} \sum_{m=-l}^{l} \int_{\mathbb{R}^2} d\boldsymbol{\nu}\, \mathbf{E}_l^m(\boldsymbol{\nu}) \left[\int_{\mathbb{S}^2} d\hat{\mathbf{s}}_o \int_{\mathbb{R}^2} d\mathbf{r}_o\, \boldsymbol{\mu}(\mathbf{r}_o, \hat{\mathbf{s}}_o) y_l^m(\hat{\mathbf{s}}_o)\, \mathrm{e}^{-i2\pi M\mathbf{r}_o\cdot\boldsymbol{\nu}} \right] \mathrm{e}^{i2\pi\mathbf{r}_d\cdot\boldsymbol{\nu}}. \tag{27}$$

We recognize the term in square brackets as the spatio-angular spectrum of the object, so we define

$$\mathbf{M}_l^m(\boldsymbol{\nu}) \equiv \int_{\mathbb{S}^2} d\hat{\mathbf{s}}_o \int_{\mathbb{R}^2} d\mathbf{r}_o\, \boldsymbol{\mu}(\mathbf{r}_o, \hat{\mathbf{s}}_o) y_l^m(\hat{\mathbf{s}}_o)\, \mathrm{e}^{-i2\pi M\mathbf{r}_o\cdot\boldsymbol{\nu}}. \tag{28}$$

and write the electric field on the detector as

$$\mathbf{e}_d(\mathbf{r}_d) = \sum_{l=0}^{\infty} \sum_{m=-l}^{l} \int_{\mathbb{R}^2} d\boldsymbol{\nu}\, \mathbf{E}_l^m(\boldsymbol{\nu}) \mathbf{M}_l^m(\nu) \mathrm{e}^{i2\pi\mathbf{r}_d\cdot\boldsymbol{\nu}}. \tag{29}$$

Eq. 38 shows that the electric field on the detector can be found by resolving the object into its spatio-angular components $\mathbf{M}_l^m(\boldsymbol{\nu})$, weighting each component by $\mathbf{E}_l^m(\boldsymbol{\nu})$, then summing over all spatio-angular components. Therefore, we identify $\mathbf{E}_l^m(\boldsymbol{\nu})$ as the spatio-angular *coherent transfer function* (CTF).

In Appendix B we calculate the paraxial CTF for a single-view fluorescence microscope as

$$\mathbf{E}_l^{m(p)}(\boldsymbol{\nu}) = \begin{bmatrix} \delta(l-1, m-1) + \frac{2}{\nu_o}\frac{\mathrm{NA}}{n_o}\nu\cos\phi_\nu\delta(l-1,m) \\ \delta(l-1, m+1) + \frac{2}{\nu_o}\frac{\mathrm{NA}}{n_o}\nu\sin\phi_\nu\delta(l-1,m) \\ 0 \end{bmatrix} \Pi\left(\frac{\nu}{\nu_o}\right). \tag{30}$$

The CTF shows that single-view coherent microscopes have a spatial band limit at $\nu = \nu_o$ and an $l = 1$ angular pass band. It is useful to compare the paraxial CTF in Eq. 30 to the paraxial electric field in the back focal plane in Eq. 5. The CTF is just a rescaled version of the electric field in the back focal plane, and this leads to an extremely valuable interpretation. The CTF of a single-view fluorescence microscope is constrained to the three members of the $l = 1$ band. The value of the CTF for each m is a rescaled version of the electric field due to a single dipole oriented along one of the Cartesian axes.

At the risk of being too explicit, the $m = 1$ CTF is a rescaled version of the electric field due to a dipole oriented along the x axis, the $m = -1$ CTF is a rescaled version of the electric field due to a dipole oriented along the y axis, and the $m = 0$ CTF is a rescaled version of the electric field due to a dipole oriented along the z axis. Therefore, we can reason about the CTF by thinking about the electric field that single x-, y-, and z-oriented dipoles create in the back focal plane.

With this interpretation in mind, the form of the CTF is not surprising. Under the paraxial approximation x- and y-oriented dipoles uniformly fill the back focal plane with an electric field parallel to the dipole axis. A z-oriented dipole creates a radial electric field with linearly increasing amplitude towards the edges of the back focal plane.

The spatial band limit can be increased by increasing the NA of the microscope, so what parameter sets the angular band limit? The angular band limit in the current microscope is set by the dipole emission process—only $l = 1$ terms show up in the CTF for dipole emitters. Adding polarizing filters to the microscope will not extend the band limit of the microscope because filters only block electric fields. However, polarized illumination can be used to extend the band limit. The excitation process is completely incoherent with the emission process,

so the spatio-angular transfer functions of the two processes will multiply. We can use the multiplication rules in Appendix A to find the band limit of a new microscope that uses selective excitation.

Next we find the intensity on the detector plane $g(\mathbf{r}_d)$ by taking the modulus squared of the electric field. Using Eq. 22 we find that

$$g(\mathbf{r}_d) = |\mathbf{e}_d(\mathbf{r}_d)|^2 = \left| \int_{\mathbb{S}^2} d\hat{\mathbf{s}}_o \int_{\mathbb{R}^2} d\mathbf{r}_o \; \tilde{\mathbf{e}}_d(\mathbf{r}_d - M\mathbf{r}_o, \hat{\mathbf{s}}_o) \boldsymbol{\mu}(\mathbf{r}_o, \hat{\mathbf{s}}_o) \right|^2. \tag{31}$$

If the dipoles emit incoherently—a fair assumption for fluorescent emitters that are not within homo-FRET distance—then we can take the squared modulus of the object and CSF independently, which gives

$$g(\mathbf{r}_d) = \int_{\mathbb{S}^2} d\hat{\mathbf{s}}_o \int_{\mathbb{R}^2} d\mathbf{r}_o \; \left|\tilde{\mathbf{e}}_d(\mathbf{r}_d - M\mathbf{r}_o, \hat{\mathbf{s}}_o)\right|^2 \left|\boldsymbol{\mu}(\mathbf{r}_o, \hat{\mathbf{s}}_o)\right|^2. \tag{32}$$

We recognize that $\left|\tilde{\mathbf{e}}_d(\mathbf{r}_d - M\mathbf{r}_o, \hat{\mathbf{s}}_o)\right|^2$ is the PSF of the microscope $h(\mathbf{r}_d - M\mathbf{r}_o, \hat{\mathbf{s}}_o)$, and we introduce a new function $f(\mathbf{r}_o, \hat{\mathbf{s}}_o) \equiv \left|\boldsymbol{\mu}(\mathbf{r}_o, \hat{\mathbf{s}}_o)\right|^2$ to represent the object

$$g(\mathbf{r}_d) = \int_{\mathbb{S}^2} d\hat{\mathbf{s}}_o \int_{\mathbb{R}^2} d\mathbf{r}_o \; h(\mathbf{r}_d - M\mathbf{r}_o, \hat{\mathbf{s}}_o) f(\mathbf{r}_o, \hat{\mathbf{s}}_o). \tag{33}$$

We can interpret $f(\mathbf{r}_o, \hat{\mathbf{s}}_o)$ as the spatio-angular density of dipoles—it is a function that is proportional to the number of fluorophores at position $\mathbf{r}_o$ oriented in direction $\hat{\mathbf{s}}_o$ per unit volume per unit solid angle. Notice that h and f are scalar functions—we removed all phase information when we took the modulus squared.

We can follow our previous work with the electric field and simplify Eq. 33 by expanding the PSF in terms of spatio-angular harmonics

$$h(\mathbf{r}_d - M\mathbf{r}_o, \hat{\mathbf{s}}_o) = \sum_{l=0}^{\infty} \sum_{m=-l}^{l} \int_{\mathbb{R}^2} d\boldsymbol{\nu} \, H_l^m(\boldsymbol{\nu}) y_l^m(\hat{\mathbf{s}}_o) \, \mathrm{e}^{i2\pi(\mathbf{r}_d - M\mathbf{r}_o)\cdot\boldsymbol{\nu}}, \tag{34}$$

where $H_l^m(\boldsymbol{\nu})$ is the spatio-angular spectrum of the PSF given by

$$H_l^m(\boldsymbol{\nu}) \equiv \int_{\mathbb{S}^2} d\hat{\mathbf{s}}_o \int_{\mathbb{R}^2} d\mathbf{r}_o \, h(\mathbf{r}_d - M\mathbf{r}_o, \hat{\mathbf{s}}_o) y_l^m(\hat{\mathbf{s}}_o) \, \mathrm{e}^{-i2\pi(\mathbf{r}_d - M\mathbf{r}_o)\cdot\boldsymbol{\nu}}. \tag{35}$$

We can change variables to make this expression easier to evaluate

$$H_l^m(\boldsymbol{\nu}) \propto \int_{\mathbb{S}^2} d\hat{\mathbf{s}}_o \int_{\mathbb{R}^2} d\mathbf{r}'_d \, h(\mathbf{r}'_d, \hat{\mathbf{s}}_o) y_l^m(\hat{\mathbf{s}}_o) \, \mathrm{e}^{-i2\pi\mathbf{r}'_d\cdot\boldsymbol{\nu}}. \tag{36}$$

By plugging Eq. 34 into Eq. 33 we find that

$$g(\mathbf{r}_d) = \int_{\mathbb{S}^2} d\hat{\mathbf{s}}_o \int_{\mathbb{R}^2} d\mathbf{r}_o \left[\sum_{l=0}^{\infty} \sum_{m=-l}^{l} \int_{\mathbb{R}^2} d\boldsymbol{\nu} \, H_l^m(\boldsymbol{\nu}) y_l^m(\hat{\mathbf{s}}_o) \, \mathrm{e}^{i2\pi(\mathbf{r}_d - M\mathbf{r}_o)\cdot\boldsymbol{\nu}} \right] f(\mathbf{r}_o, \hat{\mathbf{s}}_o). \tag{37}$$

We can rearrange this equation into the following form

$$g(\mathbf{r}_d) = \sum_{l=0}^{\infty} \sum_{m=-l}^{l} \int_{\mathbb{R}^2} d\boldsymbol{\nu} \, H_l^m(\boldsymbol{\nu}) \left[\int_{\mathbb{S}^2} d\hat{\mathbf{s}}_o \int_{\mathbb{R}^2} d\mathbf{r}_o \, f(\mathbf{r}_o, \hat{\mathbf{s}}_o) y_l^m(\hat{\mathbf{s}}_o) \, \mathrm{e}^{-i2\pi M\mathbf{r}_o\cdot\boldsymbol{\nu}} \right] \mathrm{e}^{i2\pi\mathbf{r}_d\cdot\boldsymbol{\nu}}. \tag{38}$$

We recognize the term in square brackets as the spatio-angular spectrum of the object, so we define

$$F_l^m(\boldsymbol{\nu}) \equiv \int_{\mathbb{S}^2} d\hat{\mathbf{s}}_o \int_{\mathbb{R}^2} d\mathbf{r}_o \, f(\mathbf{r}_o, \hat{\mathbf{s}}_o) y_l^m(\hat{\mathbf{s}}_o) \, \mathrm{e}^{-i2\pi M\mathbf{r}_o\cdot\boldsymbol{\nu}}. \tag{39}$$

and write the intensity on the detector as

$$g(\mathbf{r}_d) = \sum_{l=0}^{\infty} \sum_{m=-l}^{l} \int_{\mathbb{R}^2} d\boldsymbol{\nu}\, H_l^m(\boldsymbol{\nu}) F_l^m(\nu) \mathrm{e}^{i2\pi \mathbf{r}_d \cdot \boldsymbol{\nu}}. \tag{40}$$

Eq. 47 shows that the intensity on the detector can be found by resolving the object into its spatio-angular component $F_l^m(\nu_o)$, weighting each component by $H_l^m(\nu_o)$, then summing over all spatio-angular components. Therefore, we identify $H_l^m(\nu_o)$ as the spatio-angular *optical transfer function* (OTF). Notice that the CSF and CTF are vector-valued functions, while the PSF and OTF are scalar-valued functions.

In Appendix C we calculate the paraxial OTF for a single-view fluorescence microscope as

$$H_l^{m(p)}(\nu) = H_0^{0(p)}(\nu)\delta(l,m) + H_2^{0(p)}(\nu)\delta(l-2,m), \tag{41}$$

$$H_0^{0(p)}(\nu) \equiv \frac{A^{(p)}(\nu) + 2B^{(p)}(\nu)}{1 + (\mathrm{NA}/n_o)^2}, \tag{42}$$

$$H_2^{0(p)}(\nu) \equiv \frac{-A^{(p)}(\nu) + 4B^{(p)}}{\sqrt{5}\left[1 + (\mathrm{NA}/n_o)^2\right]}, \tag{43}$$

where

$$A^{(p)}(\nu) = \frac{2}{\pi}\left[\arccos\left(\frac{\nu}{2\nu_o}\right) - \frac{\nu}{2\nu_o}\sqrt{1 - \left(\frac{\nu}{2\nu_o}\right)^2}\right] \Pi\left(\frac{\nu}{2\nu_o}\right), \tag{44}$$

$$B^{(p)}(\nu) = \frac{1}{\pi}\left(\frac{\mathrm{NA}}{n_o}\right)^2 \left[\arccos\left(\frac{\nu}{2\nu_o}\right) - \left[3 - 2\left(\frac{\nu}{2\nu_o}\right)^2\right] \frac{\nu}{2\nu_o}\sqrt{1 - \left(\frac{\nu}{2\nu_o}\right)^2}\right] \Pi\left(\frac{\nu}{2\nu_o}\right). \tag{45}$$

Notice that the paraxial OTF is rotationally symmetric, so we can write in terms of ν instead of the complete spatial frequency vector $\boldsymbol{\nu}$. This will not be true when we leave the paraxial approximation or add polarizing filters to the system. Also, notice that $A^{(p)}(\nu)$ is the spatial OTF for an incoherent imaging system (the Fourier transform of an Airy pattern) under the paraxial and scalar approximations [3].

If our sample consists of isotropic distributions of fluorophores only, then we can ignore the $H_2^{0(p)}(\nu)$ term in the OTF. As the NA approaches zero, $B^{(p)}(\nu)$ disappears and we recover the scalar OTF from the vector spatio-angular OTF as expected. For non-zero NA the difference between the OTF with and without the scalar approximation is $2B^{(p)}(\nu)$. We can interpret this difference as an electromagnetic correction to the scalar OTF. The correction is proportional to $(\mathrm{NA}/n_o)^2$, so it is a small term for all but high NA objectives.

Next, consider the $H_2^{0(p)}(\nu)$ term for NA approaching zero. In this limit $H_2^{0(p)}(\nu)$ approaches the isotropic scalar paraxial OTF multiplied by a factor of $-1/\sqrt{5} \approx -0.45$. We can interpret the $H_2^{0(p)}(\nu)$ term as the spatial transfer function if our object was made entirely of fluorophores distributed like the y_2^0 spherical harmonic given by $y_2^0 = \sqrt{5/16\pi}(3\cos^2\vartheta - 1)$. The y_2^0 spherical harmonic consists of positive fluorophores near the z axis and negative fluorophores near the transverse plane. All of these fluorophores contribute to the transfer function, but the negative fluorophores in the transverse plane contribute the most (fluorophores in the transverse plane emit the most radiation along the optical axis) so the total transfer function is negative.

We can use the spatio-angular OTF to derive the spatial OTF for any distribution of fluorophores. As an example, let's derive the spatial OTF for a z-oriented fluorophore. The object is $f(\mathbf{r}_o, \hat{\mathbf{s}}_o) = \delta(\mathbf{r}_o)\delta(\hat{\mathbf{s}}_o - \hat{\mathbf{z}})$. We can calculate the angular spectrum of the object as $F_l^m(\boldsymbol{\nu}) = \int_{\mathbb{R}^2} d\mathbf{r}_o \int_{\mathbb{S}^2} d\hat{\mathbf{s}}_o \delta(\hat{\mathbf{s}}_o - \hat{\mathbf{z}}) y_l^m(\hat{\mathbf{s}}_o) \mathrm{e}^{-i2\pi M \mathbf{r}_o \cdot \boldsymbol{\nu}} = y_l^m(\hat{\mathbf{z}})$. Finally, we can plug in the angular spectrum into equation 47

$$g(\mathbf{r}_d) = \sum_{l=0}^{\infty} \sum_{m=-l}^{l} \int_{\mathbb{R}^2} d\boldsymbol{\nu}\, H_l^m(\boldsymbol{\nu}) y_l^m(\hat{\mathbf{z}}) \mathrm{e}^{i2\pi \mathbf{r}_d \cdot \boldsymbol{\nu}}, \tag{46}$$

then plug in the spatio-angular OTF from Eq. 41 and evaluate the sum to find

$$g(\mathbf{r}_d) \propto \int_{\mathbb{R}^2} d\nu \, \left[H_0^0(\nu) y_0^0(\hat{\mathbf{z}}) + H_2^0(\boldsymbol{\nu}) y_2^0(\hat{\mathbf{z}})\right] \mathrm{e}^{i2\pi \mathbf{r}_d \cdot \boldsymbol{\nu}}. \tag{47}$$

So the spatial OTF for a z oriented dipole is given by

$$H_z^{(p)}(\nu) \propto \sqrt{\frac{1}{4\pi}} H_0^0(\nu) + \sqrt{\frac{5}{4\pi}} H_2^0(\nu), \tag{48}$$

$$H_z^{(p)}(\nu) = \frac{1}{2}\left(\frac{n_o}{\mathrm{NA}}\right) B^{(p)}(\nu). \tag{49}$$

The most important result is that the spatial OTF for **any** dipole distribution is a linear combination of just two OTFs—one for each spherical harmonic. The same is true for the PSFs—the PSF for any dipole distribution is a linear combination of just two PSFs.

Fig. 2 shows four important paraxial PSFs and OTFs for a microscope with NA $= 0.8$ and $n = 1.33$. Notice that the OTF for z-oriented dipoles is negative at high frequencies. An OTF that crosses zero will give a contrast inversion in a Siemens star test target. The negative OTF is a direct consequence of the donut-shaped point spread function. If we arranged a pattern of z-oriented dipoles with a sinusoid spatial frequency near the cutoff frequency, the regions of low intensity would report the positions of the fluorophores.

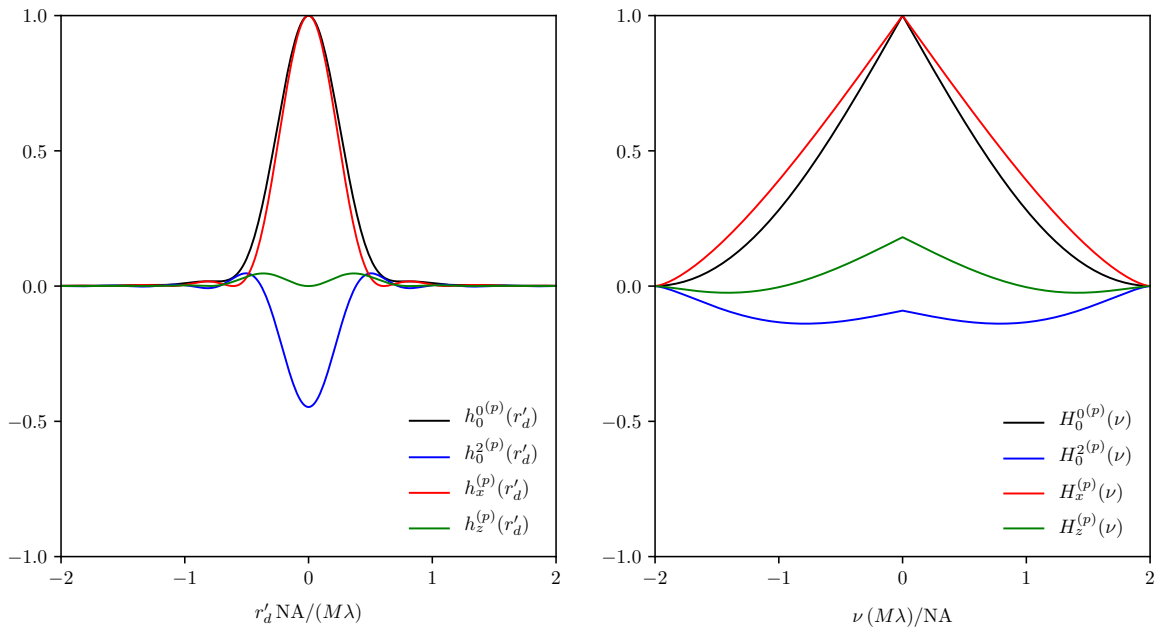

Figure 2: **Left:** Point spread functions and **Right:** optical transfer functions for a single-view fluorescence microscope with NA $= 0.8$ and $n_o = 1.33$ under the paraxial approximation. **Black:** $l = 0, m = 0$ spherical harmonic—an isotropic distribution of fluorophores. **Blue:** $l = 2, m = 0$ spherical harmonic—negative fluorophores near the transverse plane, positive fluorophores near the optical axis. **Red:** x-oriented dipole. **Green:** y-oriented dipole.

References

[1] Adam S. Backer and W. E. Moerner. Extending single-molecule microscopy using optical Fourier processing. *J. Phys. Chem. B*, 118(28):8313–8329, 2014.

[2] Lukas Novotny and Bert Hecht. *Principles of Nano-Optics*. Cambridge University Press, 2006.

[3] J.W. Goodman. *Introduction to Fourier Optics*. McGraw-Hill, 2nd edition, 1996.

[4] A. Poularikas. *Handbook of Formulas and Tables for Signal Processing*. Electrical Engineering Handbook. CRC-Press, 1998.

[5] J. Mertz. *Introduction to Optical Microscopy*. W. H. Freeman, 2009.

A Products of real spherical harmonics

The six products of $l = 1$ spherical harmonics are

$$y_1^{-1} y_1^{-1} \sqrt{\pi} = \frac{1}{2} y_0^0 - \frac{\sqrt{5}}{10} y_2^0 - \frac{\sqrt{15}}{10} y_2^2, \tag{50}$$

$$y_1^{-1} y_1^0 \sqrt{\pi} = \frac{\sqrt{15}}{10} y_2^{-1}, \tag{51}$$

$$y_1^{-1} y_1^1 \sqrt{\pi} = -\frac{\sqrt{15}}{10} y_2^{-2}, \tag{52}$$

$$y_1^0 y_1^0 \sqrt{\pi} = \frac{1}{2} y_0^0 + \frac{\sqrt{5}}{5} y_2^0, \tag{53}$$

$$y_1^0 y_1^1 \sqrt{\pi} = \frac{\sqrt{15}}{10} y_2^1, \tag{54}$$

$$y_1^1 y_1^1 \sqrt{\pi} = \frac{1}{2} y_0^0 - \frac{\sqrt{5}}{10} y_2^0 + \frac{\sqrt{15}}{10} y_2^2. \tag{55}$$

The fifteen products of $l = 2$ spherical harmonics are

$$y_2^{-2}y_2^{-2}\sqrt{\pi} = \frac{1}{2}y_0^0 - \frac{\sqrt{5}}{7}y_2^0 + \frac{1}{14}y_4^0 - \frac{\sqrt{35}}{14}y_4^4 \tag{56}$$

$$y_2^{-2}y_2^{-1}\sqrt{\pi} = -\frac{\sqrt{15}}{14}y_2^1 + \frac{\sqrt{10}}{28}y_4^1 + \frac{\sqrt{70}}{28}y_4^3 \tag{57}$$

$$y_2^{-2}y_2^{0}\sqrt{\pi} = -\frac{\sqrt{5}}{7}y_2^{-2} + \frac{\sqrt{15}}{14}y_4^{-2} \tag{58}$$

$$y_2^{-2}y_2^{1}\sqrt{\pi} = -\frac{\sqrt{15}}{14}y_2^{-1} - \frac{\sqrt{70}}{28}y_4^{-3} + \frac{\sqrt{10}}{28}y_4^{-1} \tag{59}$$

$$y_2^{-2}y_2^{2}\sqrt{\pi} = \frac{\sqrt{35}}{14}y_4^{-4} \tag{60}$$

$$y_2^{-1}y_2^{-1}\sqrt{\pi} = \frac{1}{2}y_0^0 + \frac{\sqrt{5}}{14}y_2^0 - \frac{\sqrt{15}}{14}y_2^2 - \frac{2}{7}y_4^0 - \frac{\sqrt{5}}{7}y_4^2 \tag{61}$$

$$y_2^{-1}y_2^{0}\sqrt{\pi} = \frac{\sqrt{5}}{14}y_2^{-1} + \frac{\sqrt{30}}{14}y_4^{-1} \tag{62}$$

$$y_2^{-1}y_2^{1}\sqrt{\pi} = -\frac{\sqrt{15}}{14}y_2^{-2} - \frac{\sqrt{5}}{7}y_4^{-2} \tag{63}$$

$$y_2^{-1}y_2^{2}\sqrt{\pi} = -\frac{\sqrt{15}}{14}y_2^{-1} + \frac{\sqrt{70}}{28}y_4^{-3} + \frac{\sqrt{10}}{28}y_4^{-1} \tag{64}$$

$$y_2^{0}y_2^{0}\sqrt{\pi} = \frac{1}{2}y_0^0 + \frac{\sqrt{5}}{7}y_2^0 + \frac{3}{7}y_4^0 \tag{65}$$

$$y_2^{0}y_2^{1}\sqrt{\pi} = \frac{\sqrt{5}}{14}y_2^1 + \frac{\sqrt{30}}{14}y_4^1 \tag{66}$$

$$y_2^{0}y_2^{2}\sqrt{\pi} = -\frac{\sqrt{5}}{7}y_2^2 + \frac{\sqrt{15}}{14}y_4^2 \tag{67}$$

$$y_2^{1}y_2^{1}\sqrt{\pi} = \frac{1}{2}y_0^0 + \frac{\sqrt{5}}{14}y_2^0 + \frac{\sqrt{15}}{14}y_2^2 - \frac{2}{7}y_4^0 + \frac{\sqrt{5}}{7}y_4^2 \tag{68}$$

$$y_2^{1}y_2^{2}\sqrt{\pi} = \frac{\sqrt{15}}{14}y_2^1 - \frac{\sqrt{10}}{28}y_4^1 + \frac{\sqrt{70}}{28}y_4^3 \tag{69}$$

$$y_2^{2}y_2^{2}\sqrt{\pi} = \frac{1}{2}y_0^0 - \frac{\sqrt{5}}{7}y_2^0 + \frac{1}{14}y_4^0 + \frac{\sqrt{35}}{14}y_4^4 \tag{70}$$

B Paraxial coherent transfer function

In this appendix we calculate the paraxial CTF for a single-view fluorescence microscope. We start by plugging Eq. 13 (the paraxial CSF) into Eq. 25

$$\mathbf{E}_l^{m\,(p)}(\boldsymbol{\nu}) \propto \int_{\mathbb{S}^2} d\hat{\mathbf{s}}_o \int_{\mathbb{R}^2} d\mathbf{r}'_d \begin{bmatrix} a^{(p)}(r'_d)y_1^1(\hat{\mathbf{s}}_o) + 2ib^{(p)}(r'_d)\cos\phi'_d y_1^0(\hat{\mathbf{s}}_o) \\ a^{(p)}(r'_d)y_1^{-1}(\hat{\mathbf{s}}_o) + 2ib^{(p)}(r'_d)\sin\phi'_d y_1^0(\hat{\mathbf{s}}_o) \\ 0 \end{bmatrix} y_l^m(\hat{\mathbf{s}}_o)\, \mathrm{e}^{-i2\pi\mathbf{r}'_d\cdot\boldsymbol{\nu}}. \tag{71}$$

We split the integral into two parts by writing

$$\mathbf{E}_l^{m\,(p)}(\boldsymbol{\nu}) \propto \int_{\mathbb{S}^2} d\hat{\mathbf{s}}_o\, \mathbf{E}^{(p)}(\boldsymbol{\nu};\hat{\mathbf{s}}_o) y_l^m(\hat{\mathbf{s}}_o), \tag{72}$$

$$\mathbf{E}^{(p)}(\boldsymbol{\nu};\hat{\mathbf{s}}_o) \equiv \int_{\mathbb{R}^2} d\mathbf{r}'_d \begin{bmatrix} a^{(p)}(r'_d)y_1^1(\hat{\mathbf{s}}_o) + 2ib^{(p)}(r'_d)\cos\phi'_d y_1^0(\hat{\mathbf{s}}_o) \\ a^{(p)}(r'_d)y_1^{-1}(\hat{\mathbf{s}}_o) + 2ib^{(p)}(r'_d)\sin\phi'_d y_1^0(\hat{\mathbf{s}}_o) \\ 0 \end{bmatrix} \mathrm{e}^{-i2\pi\mathbf{r}'_d\cdot\boldsymbol{\nu}}. \tag{73}$$

Substituting $a^{(p)}(r'_d)$ and $b^{(p)}(r'_d)$ using Eq. 14 gives

$$\mathbf{E}^{(p)}(\boldsymbol{\nu};\hat{\mathbf{s}}_o) = \int_{\mathbb{R}^2} d\mathbf{r}'_d \begin{bmatrix} \frac{J_1(2\pi\nu_o r'_d)}{\pi\nu_o r'_d} y_1^m(\hat{\mathbf{s}}_o) + 2i\frac{\mathrm{NA}}{n_o}\left[\frac{J_2(2\pi\nu_o r'_d)}{\pi\nu_o r'_d}\right]\cos\phi'_d y_1^0(\hat{\mathbf{s}}_o) \\ \frac{J_1(2\pi\nu_o r'_d)}{\pi\nu_o r'_d} y_1^{-1}(\hat{\mathbf{s}}_o) + 2i\frac{\mathrm{NA}}{n_o}\left[\frac{J_2(2\pi a r'_d)}{\pi\nu_o r'_d}\right]\sin\phi'_d y_1^0(\hat{\mathbf{s}}_o) \\ 0 \end{bmatrix} \mathrm{e}^{-i2\pi\mathbf{r}'_d\cdot\boldsymbol{\nu}}. \tag{74}$$

We can rewrite this in terms of three two-dimensional Fourier transforms

$$\mathbf{E}^{(p)}(\boldsymbol{\nu};\hat{\mathbf{s}}_o) \propto \begin{bmatrix} t_1(\boldsymbol{\nu}) y_1^1(\hat{\mathbf{s}}_o) + t_2(\boldsymbol{\nu}) y_1^0(\hat{\mathbf{s}}_o) \\ t_1(\boldsymbol{\nu}) y_1^{-1}(\hat{\mathbf{s}}_o) + t_3(\boldsymbol{\nu}) y_1^0(\hat{\mathbf{s}}_o) \\ 0 \end{bmatrix} \tag{75}$$

where

$$t_1(\boldsymbol{\nu}) \equiv \frac{1}{\pi\nu_o}\int_{\mathbb{R}^2} d\mathbf{r}'_d \frac{J_1(2\pi\nu_o r'_d)}{r'_d}\mathrm{e}^{-i2\pi\mathbf{r}'_d\cdot\boldsymbol{\nu}}, \tag{76}$$

$$t_2(\boldsymbol{\nu}) \equiv \frac{2i}{\pi\nu_o}\frac{\mathrm{NA}}{n_o}\int_{\mathbb{R}^2} d\mathbf{r}'_d \frac{J_2(2\pi\nu_o r'_d)}{r'_d}\cos\phi'_d\,\mathrm{e}^{-i2\pi\mathbf{r}'_d\cdot\boldsymbol{\nu}}, \tag{77}$$

$$t_3(\boldsymbol{\nu}) \equiv \frac{2i}{\pi\nu_o}\frac{\mathrm{NA}}{n_o}\int_{\mathbb{R}^2} d\mathbf{r}'_d \frac{J_2(2\pi\nu_o r'_d)}{r'_d}\sin\phi'_d\,\mathrm{e}^{-i2\pi\mathbf{r}'_d\cdot\boldsymbol{\nu}}. \tag{78}$$

All three of the functions to be transformed are separable in polar coordinates, so we can rewrite the Fourier transform as a sum of weighted Hankel transforms [3]. In general, if a function $g(r,\theta)$ is separable in polar coordinates then we can rewrite it as $g(r,\theta) = g_R(r)g_\Theta(\theta)$ and its two-dimensional Fourier transform is given by

$$\mathcal{F}\{g(r,\theta)\} = \sum_{k=-\infty}^{\infty} c_k(-i)^k \mathrm{e}^{ik\phi}\mathcal{H}_k\{g_R(r)\} \tag{79}$$

where

$$c_k = \frac{1}{2\pi}\int_0^{2\pi} d\theta\, g_\Theta(\theta)\mathrm{e}^{-ik\theta} \tag{80}$$

and $\mathcal{H}_k\{\}$ is the Hankel transform of order k given by

$$\mathcal{H}_k\{g_R(r)\} = 2\pi\int_0^\infty dr\, r g_R(r) J_k(2\pi r\nu). \tag{81}$$

First, we evaluate $t_1(\boldsymbol{\nu})$. The Fourier transform will be in polar coordinates, so we define polar coordinates in frequency space as $\boldsymbol{\nu} \equiv \nu\cos\phi_\nu\hat{\mathbf{x}} + \nu\sin\phi_\nu\hat{\mathbf{y}} \equiv \nu_x\hat{\mathbf{x}} + \nu_y\hat{\mathbf{y}}$. The angular part of $J_z(\nu_o r'_d)/r'_d$ is a constant, so $c_k = \delta(k)$ which means we only need to evaluate the zero-order Hankel transform

$$t_1(\boldsymbol{\nu}) = \frac{1}{\pi\nu_o}\mathcal{H}_0\left\{\frac{J_1(2\pi\nu_o r'_d)}{r'_d}\right\}. \tag{82}$$

From tabulated Hankel transforms we find that

$$\mathcal{H}_\mu\left\{\frac{J_{\mu+1}(2\pi\nu_o r'_d)}{r'_d}\right\} = \frac{1}{2\pi}\nu_o^{-\mu-1}\nu^\mu\,\Pi\left(\frac{\nu}{a}\right) \tag{83}$$

when $\nu_o > 0$ and $\mathrm{Re}(\mu) > -\frac{3}{2}$ [4]. Applying this result we find that

$$t_1(\boldsymbol{\nu}) = \frac{1}{2\pi^2\nu_o^2}\,\Pi\left(\frac{\nu}{\nu_o}\right). \tag{84}$$

To evaluate $t_2(\boldsymbol{\nu})$ and $t_3(\boldsymbol{\nu})$ we need to be careful with the angular part. For $t_2(\boldsymbol{\nu})$ the angular part of the function is $\cos\phi'_d = \frac{1}{2}\left(e^{i\phi'_d} + e^{-i\phi'_d}\right)$. Therefore, $c_k = \frac{1}{2}\delta(k-1) + \frac{1}{2}\delta(k+1)$ and we have to evaluate two Hankel transforms given by

$$t_2(\boldsymbol{\nu}) = \frac{2i}{\pi\nu_o}\frac{\mathrm{NA}}{n_o}\left[ie^{-i\phi_\nu}\mathcal{H}_{-1}\left\{\frac{J_2(2\pi\nu_o r'_d)}{\pi\nu_o r'_d}\right\} - ie^{i\phi_\nu}\mathcal{H}_1\left\{\frac{J_2(2\pi\nu_o r'_d)}{\pi a r'_d}\right\}\right]. \tag{85}$$

To put the Hankel transforms in the form of Eq. 83 we apply $\mathcal{H}_\mu = (-1)^\mu\mathcal{H}_{-\mu}$ to get

$$t_2(\boldsymbol{\nu}) = \frac{2i}{\pi\nu_o}\frac{\mathrm{NA}}{n_o}\left[-ie^{-i\phi_\nu}\mathcal{H}_1\left\{\frac{J_2(2\pi\nu_o r'_d)}{\pi\nu_o r'_d}\right\} - ie^{i\phi_\nu}\mathcal{H}_1\left\{\frac{J_2(2\pi\nu_o r'_d)}{\pi\nu_o r'_d}\right\}\right]. \tag{86}$$

Applying Eq. 83 and simplifying gives

$$t_2(\boldsymbol{\nu}) = \frac{1}{\pi^2\nu_o^3}\frac{\mathrm{NA}}{n_o}\nu(e^{-i\phi_\nu} + e^{i\phi_\nu})\,\Pi\left(\frac{\nu}{\nu_o}\right) \tag{87}$$

Finally,

$$t_2(\boldsymbol{\nu}) = \frac{1}{\pi^2\nu_o^3}\frac{\mathrm{NA}}{n_o}\nu\cos\phi_\nu\,\Pi\left(\frac{\nu}{a}\right) \tag{88}$$

Similarly,

$$t_3(\boldsymbol{\nu}) = \frac{1}{\pi^2\nu_o^3}\frac{\mathrm{NA}}{n_o}\nu\sin\phi_\nu\,\Pi\left(\frac{\nu}{a}\right) \tag{89}$$

Plugging Eqs. 84, 88, and 89 into Eq. 75 and normalizing gives

$$\mathbf{E}^{(p)}(\boldsymbol{\nu};\hat{\mathbf{s}}_o) = \begin{bmatrix} y_1^1(\hat{\mathbf{s}}_o) + \frac{2}{\nu_o}\frac{\mathrm{NA}}{n_o}\nu\cos\phi_\nu y_1^0(\hat{\mathbf{s}}_o) \\ y_1^{-1}(\hat{\mathbf{s}}_o) + \frac{2}{\nu_o}\frac{\mathrm{NA}}{n_o}\nu\sin\phi_\nu y_1^0(\hat{\mathbf{s}}_o) \\ 0 \end{bmatrix}\,\Pi\left(\frac{\nu}{\nu_o}\right). \tag{90}$$

Finally, we find the paraxial CTF by evaluating the angular integral in Eq. 73

$$\mathbf{E}_l^{m(p)}(\boldsymbol{\nu}) = \begin{bmatrix} \delta(l-1,m-1) + \frac{2}{\nu_o}\frac{\mathrm{NA}}{n_o}\nu\cos\phi_\nu\delta(l-1,m) \\ \delta(l-1,m+1) + \frac{2}{\nu_o}\frac{\mathrm{NA}}{n_o}\nu\sin\phi_\nu\delta(l-1,m) \\ 0 \end{bmatrix}\,\Pi\left(\frac{\nu}{\nu_o}\right). \tag{91}$$

C Paraxial optical transfer function

In this appendix we calculate the paraxial OTF for a single-view fluorescence microscope. We start with Eq. 36

$$H_l^{m(p)}(\boldsymbol{\nu}) \propto \int_{\mathbb{S}^2} d\hat{\mathbf{s}}_o \int_{\mathbb{R}^2} d\mathbf{r}'_d\, h^{(p)}(\mathbf{r}'_d,\hat{\mathbf{s}}_o) y_l^m(\hat{\mathbf{s}}_o)\,\mathrm{e}^{-i2\pi\mathbf{r}'_d\cdot\boldsymbol{\nu}}. \tag{92}$$

where the paraxial PSF is given by Eq. 21

$$h^{(p)}(\mathbf{r}'_d,\hat{\mathbf{s}}_o) = h_0^{0(p)}(\mathbf{r}'_d)y_0^0(\hat{\mathbf{s}}_o) + h_2^{0(p)}(\mathbf{r}'_d)y_2^0(\hat{\mathbf{s}}_o), \tag{93}$$

$$h_0^{0(p)}(\mathbf{r}'_d) \equiv {a^{(p)}}^2(r'_d) + 2{b^{(p)}}^2(r'_d), \tag{94}$$

$$h_2^{0(p)}(\mathbf{r}'_d) \equiv \frac{1}{\sqrt{5}}\left[-{a^{(p)}}^2(r'_d) + 4{b^{(p)}}^2(r'_d)\right]. \tag{95}$$

Plugging Eq. 94 into Eq. 92 and evaluating the angular integral gives

$$H_l^{m(p)}(\boldsymbol{\nu}) \propto \int_{\mathbb{R}^2} d\mathbf{r}'_d\,\left[h_0^{0(p)}(\mathbf{r}'_d)\delta(l,m) + h_2^{0(p)}(\mathbf{r}'_d)\delta(l-2,m)\right]\mathrm{e}^{-i2\pi\mathbf{r}'_d\cdot\boldsymbol{\nu}}. \tag{96}$$

Using the operator notation $\mathcal{F}_2\{f(\mathbf{r})\} = \int_{\mathbb{R}^2} d\mathbf{r}\{f(\mathbf{r})\}\mathrm{e}^{-i2\pi\mathbf{r}\cdot\boldsymbol{\nu}}$, we can rewrite Eq. 96 as

$$H_l^{m(p)}(\boldsymbol{\nu}) \propto \mathcal{F}_2\{h_0^{0(p)}(\mathbf{r}'_d)\delta(l,m) + h_2^{0(p)}(\mathbf{r}'_d)\delta(l-2,m)\}, \tag{97}$$

$$H_l^{m(p)}(\boldsymbol{\nu}) \propto \left[\mathcal{F}_2\left\{{a^{(p)}}^2(r'_d)\right\} + 2\mathcal{F}_2\left\{{b^{(p)}}^2(r'_d)\right\}\right]\delta(l,m) + \tag{98}$$

$$\left[-\mathcal{F}_2\left\{{a^{(p)}}^2(r'_d)\right\} + 4\mathcal{F}_2\left\{{b^{(p)}}^2(r'_d)\right\}\right]\delta(l-2,m). \tag{99}$$

To calculate $\mathcal{F}_2\left\{{a^{(p)}}^2(r'_d)\right\}$ we can use the autocorrelation theorem [3] p

$$\mathcal{F}_2\left\{f^2(r)\right\} = \mathcal{F}_2\left\{f(r)\right\} \star_2 \mathcal{F}\left\{f(r)\right\}, \tag{100}$$

where $\star_2$ denotes a two-dimensional autocorrelation. We can rewrite $\mathcal{F}_2\left\{{a^{(p)}}^2(r'_d)\right\}$ as

$$\mathcal{F}_2\left\{{a^{(p)}}^2(r'_d)\right\} = \mathcal{F}_2\left\{\frac{J_1(2\pi\nu_o r'_d)}{\pi\nu_o r'_d}\right\} \star_2 \mathcal{F}_2\left\{\frac{J_1(2\pi\nu_o r'_d)}{\pi\nu_o r'_d}\right\}. \tag{101}$$

Next, we notice that the two-dimensional Fourier transform is radially symmetric, so it can be written as a zero-order Hankel transform

$$\mathcal{F}_2\left\{{a^{(p)}}^2(r'_d)\right\} = \mathcal{H}_0\left\{\frac{J_1(2\pi\nu_o r'_d)}{\pi\nu_o r'_d}\right\} \star_2 \mathcal{H}_0\left\{\frac{J_1(2\pi\nu_o r'_d)}{\pi\nu_o r'_d}\right\}, \tag{102}$$

where the k-order Hankel transform is defined as

$$\mathcal{H}_k\left\{f(r)\right\} = 2\pi\int_0^\infty dr\, r f(r) J_k(2\pi r\nu). \tag{103}$$

Finally, we can apply the following Hankel transform identity

$$\mathcal{H}_k\left\{\frac{J_{k+1}(2\pi\nu_o r'_d)}{\pi\nu_o r'_d}\right\} = \frac{2\nu^k}{\nu_o^{k+1}}\,\Pi\left(\frac{\nu}{\nu_o}\right), \tag{104}$$

when $\nu_o > 0$ and $\mathrm{Re}(k) > -\frac{3}{2}$ [4] which gives

$$\mathcal{F}_2\left\{{a^{(p)}}^2(r'_d)\right\} = \left[\frac{2}{\nu_o}\Pi\left(\frac{\nu}{\nu_o}\right)\right] \star_2 \left[\frac{2}{\nu_o}\Pi\left(\frac{\nu}{\nu_o}\right)\right], \tag{105}$$

$$\mathcal{F}_2\left\{{a^{(p)}}^2(r'_d)\right\} = \frac{4}{\nu_o^2}\left[\Pi\left(\frac{\nu}{\nu_o}\right)\right] \star_2 \left[\Pi\left(\frac{\nu}{\nu_o}\right)\right]. \tag{106}$$

The autocorrelation is a geometry problem of finding the area of overlap of two displaced circles. Using the geometric construction in Fig. 3 we find that

$$\mathcal{F}_2\left\{{a^{(p)}}^2(r'_d)\right\} = \frac{16}{\nu_o^2}\left[\left(\int_0^{\nu_o} d\tau\,\tau \int_0^{\arccos\left(\frac{\nu}{2\nu_o}\right)} d\phi_\tau\right) - \left(\int_0^{\nu/2} d\tau_x \int_0^{\tau_x\frac{2\nu_o}{\nu}\sqrt{1-\left(\frac{\nu}{2\nu_o}\right)^2}} d\tau_y\right)\right]\Pi\left(\frac{\nu}{2\nu_o}\right), \tag{107}$$

$$\mathcal{F}_2\left\{{a^{(p)}}^2(r'_d)\right\} = \frac{16}{\nu_o^2}\left[\left(\int_0^{\nu_o} d\tau\,\tau\arccos\left(\frac{\nu}{2\nu_o}\right)\right) - \left(\int_0^{\nu/2} d\tau_x\tau_x\frac{2\nu_o}{\nu}\sqrt{1-\left(\frac{\nu}{2\nu_o}\right)^2}\right)\right]\Pi\left(\frac{\nu}{2\nu_o}\right), \tag{108}$$

$$\mathcal{F}_2\left\{{a^{(p)}}^2(r'_d)\right\} = 8\left[\arccos\left(\frac{\nu}{2\nu_o}\right) - \frac{\nu}{2\nu_o}\sqrt{1-\left(\frac{\nu}{2\nu_o}\right)^2}\right]\Pi\left(\frac{\nu}{2\nu_o}\right). \tag{109}$$

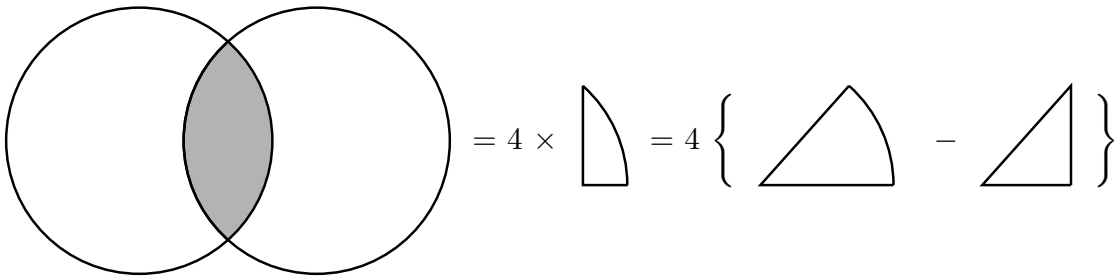

Figure 3: Geometric construction for evaluating $A^{(p)}(\boldsymbol{\nu})$ and $B^{(p)}(\boldsymbol{\nu})$. We need to find the boundaries of integration for the overlapping region of two circles with radius ν_o and distance ν between their centers. The region is given by four times the difference in area between a sector of angle $\arccos\left(\frac{\nu}{2\nu_o}\right)$ and a triangle with base $\nu/2$ and hypotenuse ν_o.

Next, we calculate $\mathcal{F}_2\left\{{b^{(p)}}^2(r'_d)\right\}$. If we follow the same steps as we did for $\mathcal{F}_2\left\{{a^{(p)}}^2(r'_d)\right\}$, we will reach a dead end because there is no Hankel transform identity that we can use. Instead, we rewrite $\mathcal{F}_2\left\{{b^{(p)}}^2(r'_d)\right\}$ in the following way so that we can use the Hankel transform identity in Eq. 104

$$\mathcal{F}_2\left\{{b^{(p)}}^2(r'_d)\right\} = \mathcal{F}_2\left\{{b^{(p)}}^2(r'_d)\cos^2(\phi'_d)\right\} + \mathcal{F}_2\left\{{b^{(p)}}^2(r'_d)\cos^2(\phi'_d)\right\}. \tag{110}$$

Now we apply the autocorrelation theorem

$$\mathcal{F}_2\left\{{b^{(p)}}^2(r'_d)\right\} = \left[\mathcal{F}_2\left\{b^{(p)}(r'_d)\cos(\phi'_d)\right\} \star_2 \mathcal{F}_2\left\{b^{(p)}(r'_d)\cos(\phi'_d)\right\}\right] + \left[\mathcal{F}_2\left\{b^{(p)}(r'_d)\sin(\phi'_d)\right\} \star_2 \mathcal{F}_2\left\{b^{(p)}(r'_d)\sin(\phi'_d)\right\}\right]. \tag{111}$$

The two autocorrelated Fourier transforms are separable in polar coordinates, so they can be expanded in terms of Hankel transforms [3]. In general, if a function $f(r,\theta)$ is separable in polar coordinates then we can rewrite it as $f(r,\theta) = f_R(r)f_\Theta(\theta)$ and its two-dimensional Fourier transform can be expanded in terms of Hankel transforms using

$$\mathcal{F}\{f(r,\theta)\} = \sum_{k=-\infty}^{\infty} c_k(-i)^k \mathrm{e}^{ik\phi}\mathcal{H}_k\{f_R(r)\}, \tag{112}$$

where

$$c_k = \frac{1}{2\pi}\int_0^{2\pi} d\theta\, f_\Theta(\theta)\mathrm{e}^{-ik\theta}. \tag{113}$$

Applying the Hankel transform expansion to $\mathcal{F}_2\left\{b^{(p)}(r'_d)\cos(\phi'_d)\right\}$ gives

$$\mathcal{F}_2\left\{b^{(p)}(r'_d)\cos(\phi'_d)\right\} = i\mathrm{e}^{i\phi_\nu}\mathcal{H}_{-1}\{b^{(p)}(r'_d)\} - i\mathrm{e}^{-i\phi_\nu}\mathcal{H}_1\{b^{(p)}(r'_d)\}. \tag{114}$$

Next, we apply the identity $\mathcal{H}_\mu = (-1)^\mu\mathcal{H}_{-\mu}$ and simplify

$$\mathcal{F}_2\left\{b^{(p)}(r'_d)\cos(\phi'_d)\right\} = \frac{i\cos\phi_\nu}{2}\mathcal{H}_1\{b^{(p)}(r'_d)\}. \tag{115}$$

Next, we evaluate the Hankel transform using Eq. 104

$$\mathcal{H}_1\{b^{(p)}(r'_d)\} = \mathcal{H}_1\left\{\frac{J_2(2\pi\nu_o r'_d)}{\pi\nu_o r'_d}\right\} = \left(\frac{\mathrm{NA}}{n_o}\right)\frac{2\nu}{\nu_o^2}\,\Pi\left(\frac{\nu}{\nu_o}\right). \tag{116}$$

Therefore,

$$\mathcal{F}_2\left\{b^{(p)}(r'_d)\cos(\phi'_d)\right\} = \left(\frac{\mathrm{NA}}{n_o}\right)\frac{i\nu\cos\phi_\nu}{\nu_o^2}\,\Pi\left(\frac{\nu}{\nu_o}\right) = \left(\frac{\mathrm{NA}}{n_o}\right)\frac{i\nu_x}{\nu_o^2}\,\Pi\left(\frac{\nu}{\nu_o}\right). \tag{117}$$

Similarly,

$$\mathcal{F}_2\left\{b^{(p)}(r'_d)\sin(\phi'_d)\right\} = \left(\frac{\mathrm{NA}}{n_o}\right)\frac{i\nu\sin\phi_\nu}{\nu_o^2}\,\Pi\left(\frac{\nu}{\nu_o}\right) = \left(\frac{\mathrm{NA}}{n_o}\right)\frac{i\nu_y}{\nu_o^2}\,\Pi\left(\frac{\nu}{\nu_o}\right). \tag{118}$$

Now we can plug these back in to the autocorrelation in Eq. 111

$$\mathcal{F}_2\left\{{b^{(p)}}^2(r'_d)\right\} = -\left(\frac{\mathrm{NA}}{n_o}\right)^2\frac{1}{\nu_0^4}\left\{\left[\nu_x\,\Pi\left(\frac{\nu}{\nu_o}\right)\right]\star_2\left[\nu_x\,\Pi\left(\frac{\nu}{\nu_o}\right)\right]\right\} - \left(\frac{\mathrm{NA}}{n_o}\right)^2\frac{1}{\nu_0^4}\left\{\left[\nu_y\,\Pi\left(\frac{\nu}{\nu_o}\right)\right]\star_2\left[\nu_y\,\Pi\left(\frac{\nu}{\nu_o}\right)\right]\right\}. \tag{119}$$

These autocorrelations can be evaluated by finding the weighted area of overlap of two circles. Neither of the autocorrelations is radially symmetric, but we know that their sum must be radially symmetric because ${b^{(p)}}^2(r'_d)$ is radially symmetric. We recognize that the first autocorrelation is largest for shifts along the x axis and smallest for shifts along the y axis with a smooth $\cos^2\phi_\nu$ weighting between the two extremes. The same is true for the second autocorrelation except with the x and y axes exchanged and a $\sin^2\phi_\nu$ weighting between the two extremes. Therefore, the sum of the two autocorrelations can be rewritten as the sum of either autocorrelation shifted along the x axis and the y axis

$$\mathcal{F}_2\left\{{b^{(p)}}^2(r'_d)\right\} = -\left(\frac{\mathrm{NA}}{n_o}\right)^2\frac{1}{\nu_0^4}\left\{\left[\nu_x\,\Pi\left(\frac{\nu}{\nu_o}\right)\right]\star_2^x\left[\nu_x\,\Pi\left(\frac{\nu}{\nu_o}\right)\right]\right\} - \left(\frac{\mathrm{NA}}{n_o}\right)^2\frac{1}{\nu_0^4}\left\{\left[\nu_x\,\Pi\left(\frac{\nu}{\nu_o}\right)\right]\star_2^y\left[\nu_x\,\Pi\left(\frac{\nu}{\nu_o}\right)\right]\right\}. \tag{120}$$

where $\star_2^x$ denotes a two-dimensional autocorrelation for shifts along the x axis.

We can use the same limits of integration as we did previously, but we need to include a weighted integrand. First, we evaluate the autocorrelation for shifts along the x-axis

$$\frac{-1}{\nu_0^4}\left\{\left[\nu_x\,\Pi\left(\frac{\nu}{\nu_o}\right)\right]\star_2^x\left[\nu_x\,\Pi\left(\frac{\nu}{\nu_o}\right)\right]\right\} = \tag{121}$$

$$= \frac{-4}{\nu_o^4}\left[\int_0^{\nu_o} d\tau\,\tau\int_0^{\arccos\left(\frac{\nu}{2\nu_o}\right)} d\phi_\tau(-\tau^2\cos^2\phi_\tau + \nu\tau\cos\phi_\tau) - \int_0^{\nu/2} d\tau_x\int_0^{\tau_x\frac{2\nu_o}{\nu}\sqrt{1-\left(\frac{\nu}{2\nu_o}\right)^2}} d\tau_y(-\tau_x^2+\nu\tau_x)\right]\Pi\left(\frac{\nu}{2\nu_o}\right). \tag{122}$$

For the first inner integral we make use of

$$\int_0^{\arccos(z)} d\phi\cos^2\phi = \frac{1}{2}z\sqrt{1-z^2} + \frac{1}{2}\arccos(z), \tag{123}$$

$$\int_0^{\arccos(z)} d\phi\cos\phi = \sqrt{1-z^2}. \tag{124}$$

This results in

$$= \frac{-4}{\nu_o^4}\left[\int_0^{\nu_o} d\tau\, \frac{-\tau^3}{2}\left(\frac{\nu}{2\nu_o}\sqrt{1-\left(\frac{\nu}{2\nu_o}\right)^2}+\arccos\left(\frac{\nu}{2a}\right)\right)+\nu\tau^2\sqrt{1-\left(\frac{\nu}{2\nu_o}\right)}\right.$$
$$\left.-\int_0^{\nu/2} d\tau_x\left(-\tau_x^3+\nu\tau_x^2\right)\frac{2\nu_o}{\nu}\sqrt{1-\left(\frac{\nu}{2\nu_o}\right)^2}\right]\Pi\left(\frac{\nu}{2\nu_o}\right), \tag{125}$$

$$= \frac{-4}{\nu_o^4}\left[\frac{-\nu_o^4}{8}\left(\frac{\nu}{2\nu_o}\sqrt{1-\left(\frac{\nu}{2\nu_o}\right)^2}+\arccos\left(\frac{\nu}{2\nu_o}\right)\right)+\frac{2\nu_o^4}{3}\frac{\nu}{2\nu_o}\sqrt{1-\left(\frac{\nu}{2\nu_o}\right)}\right.$$
$$\left.-\frac{5\nu^2\nu_o^2}{48}\frac{\nu}{2\nu_o}\sqrt{1-\left(\frac{\nu}{2\nu_o}\right)^2}\right]\Pi\left(\frac{\nu}{2\nu_o}\right), \tag{126}$$

$$= \frac{1}{2}\left[\left(\frac{\nu}{2\nu_o}\sqrt{1-\left(\frac{\nu}{2\nu_o}\right)^2}+\arccos\left(\frac{\nu}{2\nu_o}\right)\right)-\frac{16}{3}\frac{\nu}{2\nu_o}\sqrt{1-\left(\frac{\nu}{2\nu_o}\right)}\right.$$
$$\left.+\frac{5\nu^2}{6\nu_o^2}\frac{\nu}{2\nu_o}\sqrt{1-\left(\frac{\nu}{2\nu_o}\right)^2}\right]\Pi\left(\frac{\nu}{2\nu_o}\right), \tag{127}$$

$$= \frac{1}{2}\left[\arccos\left(\frac{\nu}{2\nu_o}\right)-\left(\frac{13}{3}-\frac{5\nu^2}{6\nu_o^2}\right)\frac{\nu}{2\nu_o}\sqrt{1-\left(\frac{\nu}{2\nu_o}\right)^2}\right]\Pi\left(\frac{\nu}{2\nu_o}\right), \tag{128}$$

$$= \left[\frac{1}{2}\arccos\left(\frac{\nu}{2\nu_o}\right)-\frac{1}{6}\left[13-10\left(\frac{\nu}{2\nu_o}\right)^2\right]\frac{\nu}{2\nu_o}\sqrt{1-\left(\frac{\nu}{2\nu_o}\right)^2}\right]\Pi\left(\frac{\nu}{2\nu_o}\right). \tag{129}$$

Next, we evaluate the autocorrelation for shifts along the y-axis

$$\frac{-1}{\nu_0^4}\left\{\left[\nu_x\,\Pi\left(\frac{\nu}{\nu_o}\right)\right]\star_2^y\left[\nu_x\,\Pi\left(\frac{\nu}{\nu_o}\right)\right]\right\} = \tag{130}$$

$$= \frac{-4}{\nu_o^4}\left[\int_0^{\nu_o} d\tau\,\tau\int_0^{\arccos\left(\frac{\nu}{2\nu_o}\right)} d\phi_\tau(-\tau^2\sin^2\phi_\tau)-\int_0^{\nu/2} d\tau_x\int_0^{\tau_x\frac{2\nu_o}{\nu}\sqrt{1-\left(\frac{\nu}{2\nu_o}\right)^2}} d\tau_y(-\tau_y^2)\right]\Pi\left(\frac{\nu}{2\nu_o}\right). \tag{131}$$

For the first inner integral we make use of

$$\int_0^{\arccos(z)} d\phi\sin^2\phi = -\frac{1}{2}z\sqrt{1-z^2}+\frac{1}{2}\arccos(z). \tag{132}$$

This results in

$$= \frac{-4}{\nu_o^4}\left[\int_0^{\nu_o} d\tau\,\frac{-\tau^3}{2}\left(\frac{-\nu}{2\nu_o}\sqrt{1-\left(\frac{\nu}{2\nu_o}\right)^2}+\arccos\left(\frac{\nu}{2a}\right)\right)-\int_0^{\nu/2} d\tau_x\frac{-\tau_x^3}{3}\left(\frac{2\nu_o}{\nu}\sqrt{1-\left(\frac{\nu}{2\nu_o}\right)^2}\right)^3\right]\Pi\left(\frac{\nu}{2\nu_o}\right), \tag{133}$$

$$= \frac{-4}{\nu_o^4}\left[\frac{-\nu_o^4}{8}\left(\frac{-\nu}{2\nu_o}\sqrt{1-\left(\frac{\nu}{2\nu_o}\right)^2}+\arccos\left(\frac{\nu}{2\nu_o}\right)\right)+\frac{\nu_o^4}{12}\frac{\nu}{2\nu_o}\sqrt[3]{1-\left(\frac{\nu}{2\nu_o}\right)^2}\right]\Pi\left(\frac{\nu}{2\nu_o}\right), \tag{134}$$

$$= \left[\frac{1}{2}\arccos\left(\frac{\nu}{2\nu_o}\right)-\frac{1}{2}\frac{\nu}{2\nu_o}\sqrt{1-\left(\frac{\nu}{2\nu_o}\right)^2}-\frac{1}{3}\frac{\nu}{2\nu_o}\sqrt[3]{1-\left(\frac{\nu}{2\nu_o}\right)^2}\right]\Pi\left(\frac{\nu}{2\nu_o}\right). \tag{135}$$

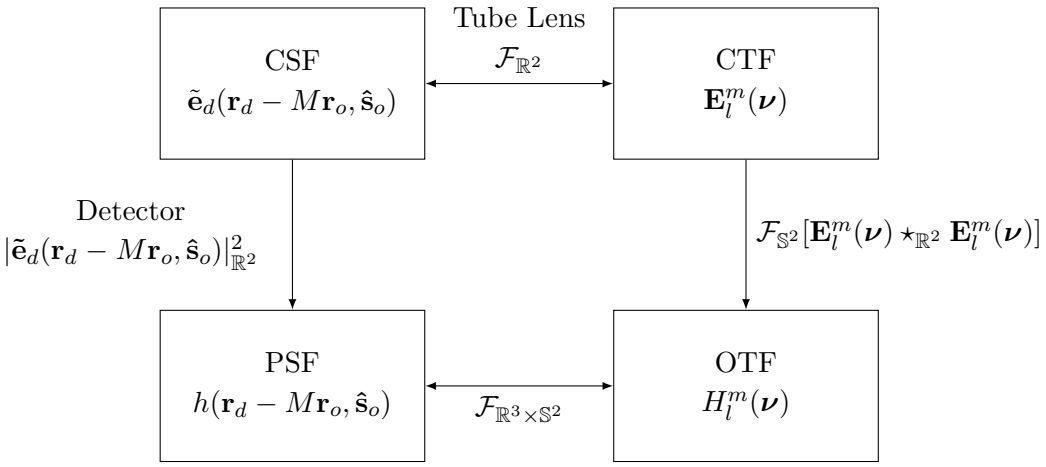

Figure 4: Summary of relationships between the CSF, CTF, PSF, and OTF where $\mathcal{F}_D$, $|\cdot|_D$, and $\star_D$ denote the Fourier transform, norm, and autocorrelation over the set D, respectively. See [3] and [5] for analogous diagrams under scalar optics approximations.

Combining the results in Eqs. 129 and 135 gives us the final Fourier transform

$$\mathcal{F}_2\left\{{b^{(p)}}^2(r'_d)\right\} = \left(\frac{\mathrm{NA}}{n_o}\right)^2 \left[\arccos\left(\frac{\nu}{2\nu_o}\right) - \frac{1}{3}\left[8 - 5\left(\frac{\nu}{2\nu_o}\right)^2\right]\frac{\nu}{2\nu_o}\sqrt{1-\left(\frac{\nu}{2\nu_o}\right)^2} - \frac{1}{3}\frac{\nu}{2\nu_o}\sqrt[3]{1-\left(\frac{\nu}{2\nu_o}\right)^2}\right]\Pi\left(\frac{\nu}{2\nu_o}\right), \tag{136}$$

$$\mathcal{F}_2\left\{{b^{(p)}}^2(r'_d)\right\} = \left(\frac{\mathrm{NA}}{n_o}\right)^2 \left[\arccos\left(\frac{\nu}{2\nu_o}\right) - \left[3 - 2\left(\frac{\nu}{2\nu_o}\right)^2\right]\frac{\nu}{2\nu_o}\sqrt{1-\left(\frac{\nu}{2\nu_o}\right)^2}\right]\Pi\left(\frac{\nu}{2\nu_o}\right). \tag{137}$$

Now that we've evaluated $\mathcal{F}_2\left\{{a^{(p)}}^2(r'_d)\right\}$ and $\mathcal{F}_2\left\{{b^{(p)}}^2(r'_d)\right\}$, we can plug the results into the following equation and we have the complete spatio-angular transfer function

$$H_l^{m(p)}(\boldsymbol{\nu}) \propto \left[\mathcal{F}_2\left\{{a^{(p)}}^2(r'_d)\right\} + 2\mathcal{F}_2\left\{{b^{(p)}}^2(r'_d)\right\}\right]\delta(l,m) + \tag{138}$$

$$\left[-\mathcal{F}_2\left\{{a^{(p)}}^2(r'_d)\right\} + 4\mathcal{F}_2\left\{{b^{(p)}}^2(r'_d)\right\}\right]\delta(l-2,m). \tag{139}$$

After refactoring and normalizing, we have the final spatio-angular transfer function

$$H_l^{m(p)}(\nu) = H_0^{0(p)}(\nu)\delta(l,m) + H_2^{0(p)}(\nu)\delta(l-2,m), \tag{140}$$

$$H_0^{0(p)}(\nu) \equiv \frac{A^{(p)}(\nu) + 2B^{(p)}(\nu)}{1 + (\mathrm{NA}/n_o)^2}, \tag{141}$$

$$H_2^{0(p)}(\nu) \equiv \frac{-A^{(p)}(\nu) + 4B^{(p)}}{\sqrt{5}\left[1 + (\mathrm{NA}/n_o)^2\right]}, \tag{142}$$

where

$$A^{(p)}(\nu) = \frac{2}{\pi}\left[\arccos\left(\frac{\nu}{2\nu_o}\right) - \frac{\nu}{2\nu_o}\sqrt{1-\left(\frac{\nu}{2\nu_o}\right)^2}\right]\Pi\left(\frac{\nu}{2\nu_o}\right), \tag{143}$$

$$B^{(p)}(\nu) = \frac{1}{\pi}\left(\frac{\mathrm{NA}}{n_o}\right)^2 \left[\arccos\left(\frac{\nu}{2\nu_o}\right) - \left[3 - 2\left(\frac{\nu}{2\nu_o}\right)^2\right]\frac{\nu}{2\nu_o}\sqrt{1-\left(\frac{\nu}{2\nu_o}\right)^2}\right]\Pi\left(\frac{\nu}{2\nu_o}\right). \tag{144}$$